Underway and Moored Methods for Improving Accuracy in Measurement of Spectral Particulate Absorption and Attenuation

WAYNE H. SLADE,* EMMANUEL BOSS,* GIORGIO DALL'OLMO,+ M. ROIS LANGNER,#,& JAMES LOFTIN,* MICHAEL J. BEHRENFELD,+ COLLIN ROESLER,@ AND TOBY K. WESTBERRY+

* *School of Marine Sciences, University of Maine Orono, Orono, Maine*
+ *Department of Botany and Plant Pathology, Oregon State University, Corvallis, Oregon*
# *Bigelow Laboratory for Ocean Sciences, West Boothbay Harbor, Maine*
@ *Department of Geology, Bowdoin College, Brunswick, Maine*

(Manuscript received 18 November 2009, in final form 18 March 2010)

ABSTRACT

Optical sensors have distinct advantages when used in ocean observatories, autonomous platforms, and on vessels of opportunity, because of their high-frequency measurements, low power consumption, and the numerous established relationships between optical measurements and biogeochemical variables. However, the issues of biofouling and instrument stability over time remain complicating factors when optical instruments are used over periods longer than several days. Here, a method for obtaining calibration-independent measurements of spectral particle absorption and attenuation is presented. Flow-through optical instrumentation is routinely diverted through a large–surface area 0.2-μm cartridge filter, allowing for the calculation of particle optical properties by differencing temporally adjacent filtered and whole water samples. This approach yields measurements that are independent of drift in instrument calibration. The method has advantages not only for coastally moored deployments, but also for applications in optically clear waters where uncertainties in instrument calibration can be a significant part of the signal measured. The differencing technique is demonstrated using WET Labs (Philomath, Oregon) ac-9 and ac-s multi- and hyperspectral absorption and attenuation meters. For the ac-s sensor, a correction scheme is discussed that utilizes the spectral shape of water absorption in the near-infrared to improve the accuracy of temperature and scattering-corrected spectra. Flow-through particulate absorption measurements are compared with discrete filter-pad measurements and are found to agree well ($R^2 = 0.77$; rmse $= 0.0174$ m^{-1}).

1. Introduction

Validation of ocean color remote sensing data products and biogeochemical model outputs is often hindered by a dearth of in situ data with high spatial and temporal coverage. This inadequacy can be addressed using shipboard flow-through systems equipped with sensors measuring appropriate parameters, which have the advantage of high-frequency measurement and low power consumption (e.g., Ainsworth 2008). For ocean color validation, the primary variables of interest are the optical absorption, attenuation, and backscattering coefficients. These quantities can be used to validate remotely sensed optical parameters and to estimate biomass and, using variable fluorescence, the physiological state of phytoplankton (e.g., Mueller et al. 2003; Behrenfeld and Boss 2003), as well as to provide constraints on particulate and dissolved pools and properties in ecosystem models (e.g., Fujii et al. 2007). Spectral particulate absorption and attenuation have also been used to derive proxies for the concentration of particulate organic carbon (Gardner et al. 1993; Bishop 1999), particulate suspended mass (Peterson 1978), an index of particulate size distribution (Boss et al. 2001), chlorophyll concentration (Bricaud et al. 1998), the presence of a variety of phytoplankton groups or pigments (e.g., Eisner et al. 2003; Schofield et al. 2004), and diver visibility (Zaneveld and Pegau 2003).

However, optical instrumentation is vulnerable to the effects of biofouling, drift in electronic circuits, and degradation of light sources, detectors, and spectral filters.

& Current affiliation: Electricity, Resources, and Building Systems Integration Center, National Renewable Energy Laboratory, Golden, Colorado.

Corresponding author address: Wayne H. Slade, 5706 Aubert Hall, University of Maine Orono, Orono, ME 04469.
E-mail: wayne.slade@gmail.com

DOI: 10.1175/2010JTECHO755.1

The fouling of optical surfaces resulting from particle accumulation and biofilm production can be minimized using a variety of techniques, such as the use of automated copper shutters that cover the optical windows when not in use (Manov et al. 2004). Drift in electronic and optical systems is usually handled by frequent (daily) calibrations with the cleanest water available (Twardowski et al. 1999). Calibration offsets are calculated by the manufacturer, in the users' laboratory, and in the field using available optically pure water sources. Such calibrations are recommended when the instrument is either shipped or transported, and periodically while deployed, to account for possible changes in optical alignment, spectral filter response, and lamp and electro-optics drift over time (e.g., Twardowski et al. 1999; Roesler and Boss 2008). For instruments deployed on either moorings or in shipboard flow-through systems, routine calibrations may not be possible because of logistical, personnel, or equipment limitations. In addition, in clear open-ocean waters, absolute calibration is difficult because in situ optical properties are often of the same order of magnitude ($<0.01\ m^{-1}$) as the instrument accuracy based on the stability of repeated pure water calibrations ($0.003\ m^{-1}$; WET Labs 2009).

When interested in optical properties of particles, differences between total and filtered measurements performed with the same instrument can be used to obtain calibration-independent properties. This idea has been used by Boss and Zaneveld (2003), Balch et al. (2004), and Boss et al. (2007) to obtain optical properties of particles near coral reefs from a diver-based package, from an in-line measurement system on a ferry, and from the ultraclear water of Crater Lake using a profiling system, respectively. In each case, the underlying assumptions are that the temporal and/or spatial variability of the dissolved properties varies little in the time between the total and dissolved measurements, and that the filter does not add or remove dissolved material.

Here, we present the latest evolution of the filtered–unfiltered differencing technique as used in shipboard and moored applications utilizing a combination of commercially available and custom-designed instrumentation. By differencing unfiltered and filtered measurements and time averaging, we obtain stable spectra on multiple-week cruises and moored deployments. In addition, spectra from the cruises show agreement with coincident filter-pad absorption measurements. When using hyperspectral (as opposed to multispectral) measurements of absorption, temperature and scattering corrections are further improved by taking advantage of the known temperature dependence of water absorption. This methodology holds promise for obtaining high-quality particulate optical properties by nonspecialists on moorings and ship-of-opportunity applications. The same methodology could also be applied to vertical profiling applications of the WET Labs (Philomath, Oregon) ac-s sensor as well.

2. Materials and procedures

In this paper we present two methods of using the differencing technique: first in an underway flow-through system on a research vessel (R/V) or ship of opportunity, and then in a fixed tripod-based application. Following a description of each of these deployment modes, a description of the absorption and attenuation measurements made with WET Labs ac-9 and ac-s sensors, within the context of the filtered/unfiltered differencing technique, is provided. Finally, a method for improving the accuracy of ac-s absorption spectra by removing dependence on correcting spectra using measured temperature data is provided.

a. Underway flow-through system

Underway flow-through particulate absorption and attenuation observations were collected on three cruises (the Equatorial Box Project: GP5-05 August–September 2005, GP1-06 January–February 2006, and GP5-06 August–September 2006) along an equatorial transect from approximately 8°N to 8°S along 140°W longitude and then east to 125°W, and from 8°S to 8°N, completing three sides of a box. During the GP5-05 and GP1-06 cruises, we used an ac-9 with the 0.2-μm cartridge filter engaged manually when on station, and also occasionally while in transit. During the GP5-06 cruise, an ac-s and automated valve system were employed.

The uncontaminated seawater supply used for the flow-through system is sourced from the ship's sea chest, with bow intake at roughly 2–5 m below the sea surface for the research vessels used during the development of the method. In the wet laboratory, the seawater supply was passed through two Vortex debubblers in series [Ocean Instrument Laboratory, Stony Brook University model VDB-1G, Stony Brook, New York]. The debubblers were added to the flow-through system after having intermittent problems with bubbles during early field testing of the system. Even with the series Vortex debubblers, bubbles remain problematic during occasional periods of high sea state in which the bow intake rises above the sea surface or is high enough to draw highly aerated seawater. Such data are easily detectable either as spikes in salinity data or as spikes in raw (or increased variance in binned) attenuation data. In practice, data for bins with variance higher than a threshold (determined from data in calm seas) are discarded in postprocessing.

After passing through the debubblers, seawater is periodically diverted by a valve through a large–surface

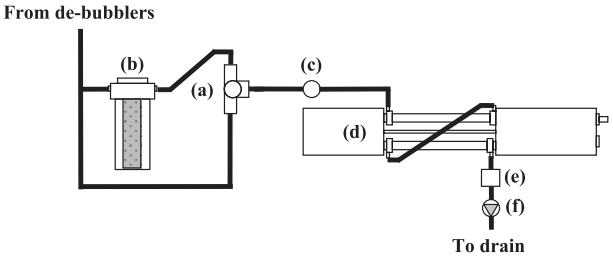

FIG. 1. Example flow-through system setup. Seawater inflow can be diverted using (a) a three-way ball valve, either (b) through a 0.2-mm filter or (d) directly to the ac-9 or ac-s instrument. (c) A stopcock or needle valve with quick-disconnect fitting is used to control flow rates to the instrument and facilitate its removal for cleaning. (e) A volume flow sensor is used to assess fouling of the filter over time. (f) A check valve ensures that no air is drawn into the instrument under a no-flow condition.

area 0.2-μm cartridge filter (the PALL AcroPak Supor Membrane was used during the early cruises, while later the GE Osmonics Memtrex NY was used), as detailed in Fig. 1. An automated valve controller, employing a programmable logic controller (PLC; Toshiba, Model T1-16) with a real-time clock–calendar and an electrically actuated three-way ball valve (Hayward Industrial Products three-way lateral ball valve, ½″ PVC, with a 24-V dc EJM series actuator), is used to control the flow. The PLC is programmed to divert seawater flow through the filter at user-programmable intervals. The latest versions of the controller include a personal computer (PC) Universal Serial Bus (USB)-connected relay and input/output (I/O) controller (ADU208, Ontrak Control Systems) connected to the electrically actuated three-way ball valve and multiple-paddle-wheel flow sensors (FPR301, Omega Engineering, Inc.). A laptop with custom software is used to interface with the controller in order to set the filter valve schedule and to log data from the flow sensors. Filter cartridges are replaced when the flow rate through the filter decreases significantly (typically after a 50% reduction in flow rate, or roughly once per week). Finally, filtered or total seawater are passed to optical instruments (such as the ac-s) via a manifold. During the cruises discussed here, optical instruments were cleaned every 1–2 days.

Data from all instruments are merged and time stamped using a WET Labs DH-4 data handler with WET Labs Archive Protocol (WAP) software. Seawater temperature and salinity (SBE-21, Sea-Bird Electronics, Bellevue, Washington), as well as GPS coordinates, are logged by the ship's computing systems and are later merged with the optical property datasets. All of the raw data are binned to 1-min intervals before postprocessing, such as the unfiltered–filtered seawater differencing and residual temperature and scattering correction, discussed below.

The various components of the flow-through system, such as the ship's pump, plumbing, debubblers, and the optical instrumentation itself, represent sources of shear within the system. Potential effects of shear on the particle suspension range from the breakage of aggregates to the destruction of individual cells, as can be the case, especially with strong impeller pumps at high flow rates. Fouling of the plumbing also represents a potential source of particulate material to the flow-through system. To verify the quality of the uncontaminated seawater supply, it is recommended that in situ optical instruments are deployed periodically during the cruise, such as by including a beam transmissometer in the ship's CTD rosette. Comparison of flow-through and rosette-mounted measurements from a dataset compiled from cruises in the equatorial Pacific, Mediterranean, and North Atlantic aboard the three different research vessels indicate good agreement between the two methods (Westberry et al. 2010; median bias of $0.0001 \pm 0.31\ m^{-1}$). However, without verification of the quality of seawater supply used in a particular application, data should be regarded with suspicion; and even when the flow-through system has been validated, the effects of particle disaggregation (and other shear effects) should be considered in data interpretation. If the quality of the ship's uncontaminated seawater supply is questioned, then it is worthwhile to consider the addition of a dedicated pump (such as a diaphragm pump) and plumbing to the flow-through system.

b. Moored system

As part of the Optics, Acoustics and Stress In Situ (OASIS) experiment, tripod-based measurements using the differencing technique were made with an ac-9 sensor that is coupled to an electrically actuated valve contained in submersible pressure housing (which was custom manufactured by WET Labs, model EBS-001, built around a Parker valve stainless steel three-way valve with a 24-V dc actuator). The tripod was located at the Woods Hole Oceanographic Institution's Martha's Vineyard Coastal Observatory (MVCO), in approximately 12-m water depth, with instruments configured to measure optical properties at 1.2 m above the bottom. The filter housing used during the deployments was drilled with large holes such that a large amount of surface area of the filter is exposed and seawater can readily be drawn through it, increasing flow rates through the filter. The instrumented tripod was connected to the shore for power and communication (through an underwater observatory node), and the actuated valve was controlled from the shore by alternately energizing power supplies connected to the valve system on a schedule, controlled using a ''cron'' script on one of the observatory's servers. Data from

the ac-9 were logged on the tripod using a custom data-logging system, and subsequently were transferred to the shore for processing. Similar to the underway system, all data are binned to 1-min intervals. The tripod also contained a number of other optical instruments, as well as a CTD for conductivity and temperature measurements.

Compared with the underway system, the logistics of maintenance become especially problematic for moored deployments, where ship and diver scheduling, as well as weather become significant challenges. These challenges are in part overcome by laying out the tripod such that the filter is easily accessible and replaceable by the diver, as part of routine maintenance in the event that scheduling or weather precluded the full recovery of the tripod.

c. *Absorption and attenuation measurements*

Absorption and attenuation measurements are made using WET Labs ac-9 or ac-s instruments, in situ absorption and attenuation meters utilizing dual-flow tubes (attenuation and absorption tubes), a collimated source lamp, and spectral bandpass filters arranged on a rotating wheel, producing absorption and attenuation spectra at multiple wavelengths in the visible through the near-infrared (NIR; Moore et al. 1997; Twardowski et al. 1999). Absorption is measured using a reflective tube and a wide-angle detector (with diffuser) and attenuation is measured using a nonreflective tube and collimated detector. The ac-9 instrument measures at nine wavelengths at a rate of 6 Hz. The ac-s is a similar design, but provides measurements at greater than 80 wavelengths using a linear variable filter, producing complete spectra at 4 Hz, nominal. Each instrument is available in 10- and 25-cm pathlength versions.

In this work, we have used either the WET Labs 25-cm pathlength ac-s or ac-9 when deploying the underway system, and the 10-cm pathlength ac-9 when deploying the bottom tripod. Both ac-9 and ac-s are calibrated at the factory to produce zero output in clean freshwater. However, field calibrations are desired in order to remove the effects of optical misalignment and instrument drift since the most recent factory or laboratory calibration.

The absorption of pure water is dependent on temperature and salinity in the red and NIR portion of the visible spectrum. In situ measurements of absorption and attenuation therefore include not only the effects of particulate and dissolved materials, but also the difference between the absorption coefficient of the water being measured and the reference water being used for instrument calibration. The change in absorption can be expressed as

$$\Delta a_{sw}(\lambda, T, S) = (T - T_{ref})\Psi_T + (S - S_{ref})\Psi_S, \quad (1)$$

where, T and S are the in situ water temperature and salinity; T_{ref} and S_{ref} are the temperature and salinity of the water used for calibration; and Ψ_T (m^{-1} °C^{-1}) and Ψ_S (m^{-1} psu^{-1}) are the temperature- and salinity-specific absorption coefficients of water (Pegau and Zaneveld 1994; Twardowski et al. 1999; Sullivan et al. 2006). Selection of the temperature- and salinity-specific absorption coefficients depends on the type of instrument used. For the ac-s measurements, we use the coefficients given in Sullivan et al. (2006), which were determined with the ac-s instrument used in our underway system, and are not applicable to the ac-9 because of differences in instrument design and the optical filter bandwidth. For the ac-9, coefficients from Pegau and Zaneveld (1994) are used.

Reflecting-tube absorption meters, such as the ac-9 and ac-s, do not collect all of the light scattered from the incident beam, causing the instruments to overestimate the absorption coefficient. In most spectrophotometers, scattering correction is accomplished by subtraction of a baseline value around 750 nm, assuming that 1) absorption is negligible in this region of the spectra, and 2) that the scattering coefficient is spectrally flat (Bricaud and Stramski 1990). For the ac-9 and ac-s, a more reasonable scattering correction scheme can be employed since the instruments also measure spectral beam attenuation. Because the spectral scattering coefficient can be determined as the difference in attenuation and absorption, the assumption that the scattering coefficient is spectrally flat is not needed. Instead, a first-order scattering coefficient is calculated as the difference of measured (and already temperature and salinity corrected) attenuation and absorption,

$$b'_p(\lambda) = c_{p,meas}(\lambda) - a_{p,meas}(\lambda). \quad (2)$$

This scattering coefficient will be slightly underestimated because the uncorrected absorption is overestimated. Absorption is corrected using the spectral shape of the first-order scattering coefficient and by assuming that absorption at a reference wavelength λ_{ref} in the near-infrared is negligible (Zaneveld et al. 1994),

$$a_p(\lambda) = a_{p,meas}(\lambda) - a_{p,meas}(\lambda_{ref})\frac{b'_p(\lambda)}{b'_p(\lambda_{ref})}. \quad (3)$$

For the ac-9, λ_{ref} = 715 nm is used, while for the ac-s, λ_{ref} = 730 nm. The choice of λ_{ref} = 730 nm was made to extend the zero absorption wavelength as far as possible into the NIR, and was found (in the context of the combined residual temperature and scattering correction) to offer the most reasonable-looking spectra in the NIR. Values higher than 730 nm were more vulnerable to

increased instrument noise in wavelengths greater than approximately 730 nm (for our instrument).

Calibration-independent particulate property measurements are made by calculating the difference of the total and filtered sea water measurements (TSW and FSW, respectively), for example, for absorption;

$$a^{\mathrm{TSW}}_{\mathrm{meas}}(\lambda) = a_{p,\mathrm{meas}}(\lambda) + a_g(\lambda) + a_{\mathrm{offset}}(\lambda) + \Delta a_{\mathrm{sw}}(\lambda, T, S)$$
$$a^{\mathrm{FSW}}_{\mathrm{meas}}(\lambda) = a_g(\lambda) + a_{\mathrm{offset}}(\lambda) + \Delta a_{\mathrm{sw}}(\lambda, T, S), \quad (4)$$

where a_g denotes dissolved absorption, $a_{p,\mathrm{meas}}$ is the measured particulate absorption (not corrected for scattering), and a_{offset} denotes the instrumental difference from water absorption at a reference temperature and with no salts.

In practice, the automated valve system is used to divert flow through the 0.2-μm filter every hour, for approximately 5–10 min. For deployments where high variability in dissolved absorption is expected, the filtered measurement interval can be reduced. Continuously logged raw data are binned to minute intervals, and $a^{\mathrm{FSW}}_{\mathrm{meas}}(\lambda)$ is linearly interpolated over time between the FWS measurements and subtracted from $a^{\mathrm{TSW}}_{\mathrm{meas}}(\lambda)$ measurements, yielding the calibration-independent particulate spectra,

$$a_{p,\mathrm{meas}}(\lambda) = a^{\mathrm{TSW}}_{\mathrm{meas}}(\lambda) - a^{\mathrm{FSW}}_{\mathrm{meas}}(\lambda),$$

which must subsequently be corrected for scattering effects. The uncorrected beam attenuation spectra is similarly calculated as $c_{p,\mathrm{meas}}(\lambda) = c^{\mathrm{TSW}}_{\mathrm{meas}}(\lambda) - c^{\mathrm{FSW}}_{\mathrm{meas}}(\lambda)$.

Since the periodic (and then interpolated) FSW measurements are subtracted from TSW samples to give the absorption resulting from particles $a_{p,\mathrm{meas}}(\lambda)$, the dependence on clean water offset and temperature and salinity corrections is, in principle, eliminated (because we are assuming that the temperature and salinity differences between TSW and FSW measurements is zero). Both the clean water offsets and temperature corrections can be sources of uncertainty in postprocessing absorption data. The uncertainty resulting from temperature (even less so for salinity) correction arises because the sensitivity of water absorption in the NIR to temperature [Eq. (1)] is approximately 0.0035 $\mathrm{m}^{-1}\,^{\circ}\mathrm{C}^{-1}$ at 715 nm (Fig. 2b). Thus, a small uncertainty (e.g., 0.1°C) in the in situ water temperature, or a change in the temperature between dissolved and total measurement, can lead to a significant uncertainty in NIR absorption. This is a twofold problem because of the uncertainty in the temperature-corrected absorption coefficient in the NIR and because the measured absorption signal in this wavelength region is used to correct absorption spectra for the effects of particle scattering within the sample volume. In field data, these uncertainties are often of the order or 0.005 m^{-1} and

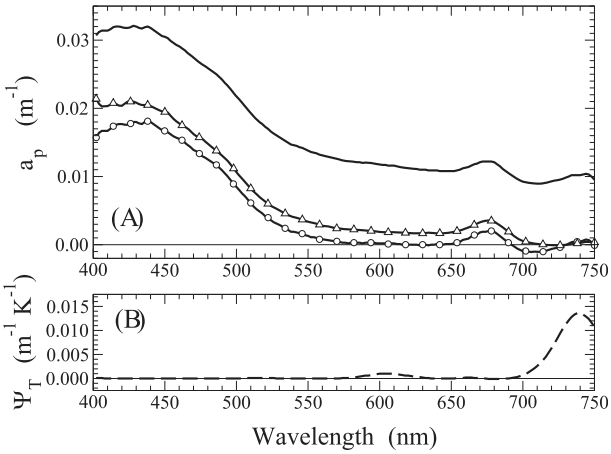

FIG. 2. (a) Example of uncorrected particulate absorption spectrum (solid line) showing a spectral anomaly between 710 and 750 nm. The continuous lines with circles and triangles represent the spectra derived from using standard correction procedures [Eq. (3)], and the residual temperature correction [Eq. (5)], respectively. The derived ΔT for this sample data was approximately 0.13°C. (b) The pure water temperature dependence $\Psi_T(\lambda)$ from Sullivan et al. (2006). Note the spectral features in Ψ_T centered near 600 and 740 nm, and note that the manufacturer-specified uncertainty is ± 0.005 m^{-1}.

can be substantial in comparison to the absorption signals in optically clear waters, which are often <0.01 m^{-1}. In addition, the independent uncertainty in clean water calibration (the stability of repeated calibrations and cleaning) is also typically of the order of 0.005 m^{-1}.

d. Residual temperature and scattering correction

Because of its strong temperature dependence, a spectral anomaly in the NIR region often becomes noticeable in highly precise absorption spectra (Fig. 2a). This anomaly is characterized by a local minimum or maximum centered near 740 nm, corresponding with the maximum in the temperature dependence of pure water absorption (a_w) in this spectral region (Fig. 2b; see also Pegau and Zaneveld 1993; Sullivan et al. 2006). The maximum becomes a minimum when the sign of the temperature change is inverted. At 740 nm, $\Delta T = 0.1$°C causes a maximal $\Delta a_w = 0.0014$ m^{-1}, which is comparable to the values of particulate absorption (a_p) at 676 nm for waters with about 0.1 mg Chl a m^{-3} (see inset in Fig. 3d). Because NIR a_p measurements are used in the scattering correction of absorption spectra (Zaneveld et al. 1994), biases in $a_p(\lambda_{\mathrm{NIR}})$ will propagate to the whole spectrum. In a worst-case scenario these biases may even result in negative a_p values (though still significantly smaller than the manufacturer-specified uncertainty) in certain parts of the spectrum (Fig. 2a). In addition, changes in temperature could also introduce spectral features in a_p

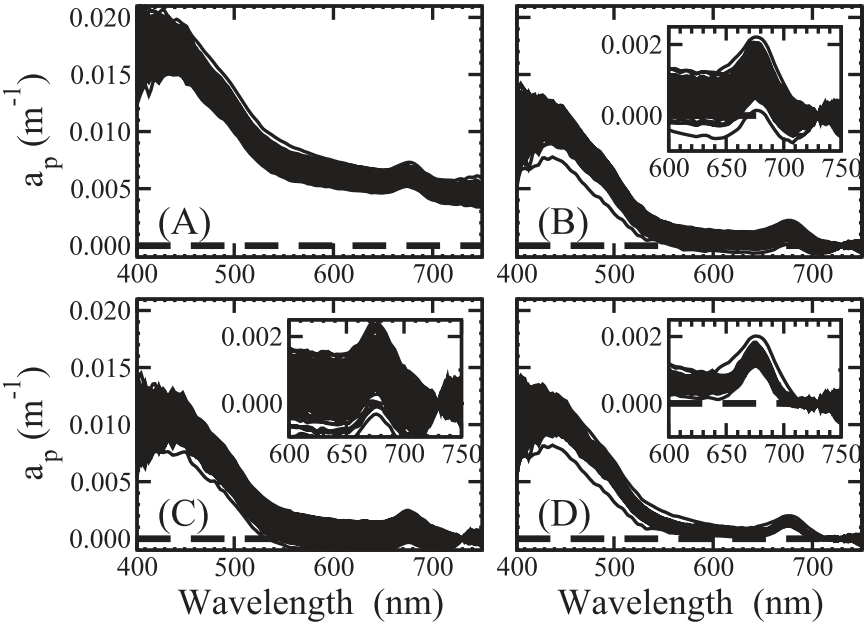

FIG. 3. (a) One-fifth of the 1-min binned, uncorrected a_p spectra recorded on day 31 of the cruise; (b) spectra with only the scattering correction applied; (c) spectra with scattering and traditional temperature and salinity corrections applied; and (d) a_p spectra corrected using Eq. (5) and the ΔT derived by minimizing Eq. (6). Insets show the red–NIR region where the effects of inaccurate ΔT are most apparent. Note the presence of negative a_p in the visible range in (b) and (c).

around 600 nm that may be taken mistakenly as phytoplankton pigment absorption peaks (Fig. 2b).

Fluctuations in sample temperature ΔT of the order of 0.1°C are expected on the short temporal and spatial scales between the filtered and total water measurements resulting from finescale natural environmental variability and to changes in sample temperature between the locations of the ac-s and thermosalinograph (TSG). Changes in salinity that are typical of our open-ocean study are on the order of 0.1 psu, and have a smaller effect on a_{sw} because the maximal changes in a_{sw} resulting from a salinity change of 0.1 psu are more than an order of magnitude smaller than the changes in a_{sw} resulting from a temperature change of 0.1°C. Thus, in this study variations in temperature were considered the main cause for the observed anomalies in $a_p(\lambda_{NIR})$.

To remove the spectral artifacts and overcome the described limitations of the differencing approach that arise because of variations in water temperature, the scattering correction of Eq. (3) is combined with a residual temperature correction accounting for the differences between the filtered and unfiltered measurements ΔT,

$$a_{p(\lambda)} = a_{p,\mathrm{meas}}(\lambda) - \Psi_T(\lambda)\Delta T - \frac{a_{p,\mathrm{meas}}(\lambda_{\mathrm{ref}}) - \Psi_T(\lambda_{\mathrm{ref}})\Delta T}{b'_p(\lambda_{\mathrm{ref}})} b'_p(\lambda). \quad (5)$$

The scattering and temperature corrections are combined because we have constraints on the true particulate absorption in the NIR. While the ΔT between TSW and FSW measurements can be derived using in-line TSG or thermistor data, in practice ΔT is often not known to have a sufficiently high enough accuracy or precision. For example, in our open-ocean campaigns, the in-line TSG was not located optimally enough to provide the high precision that is needed for scattering correction of such low-absorption waters. In such a case, assuming that a_p is spectrally flat over the NIR wavelengths (Babin and Stramski 2002), allowed us to use a spectral fitting based on Eq. (5) to determine ΔT, and concurrently to correct for the effects of temperature difference between TSW and FSW samples and for particle scattering. The fitting procedure is applied over the range of wavelengths in the NIR containing the spectral anomaly λ_{NIR}, and varies ΔT in order to minimize the variance in $a_p(\lambda_{NIR})$. The specific cost function to be minimized is

$$\chi = \sum_{\lambda_{\mathrm{NIR}}} \left| a_{p,\mathrm{meas}}(\lambda_{\mathrm{NIR}}) - \Psi_T(\lambda_{\mathrm{NIR}})\Delta T - \frac{a_{p,\mathrm{meas}}(\lambda_{\mathrm{ref}}) - \Psi_T(\lambda_{\mathrm{ref}})\Delta T}{b'_p(\lambda_{\mathrm{ref}})} b'_p(\lambda_{\mathrm{NIR}}) \right|, \quad (6)$$

where $\lambda_{NIR} = [710...750]$ nm and $\lambda_{ref} = 730$ nm. Note that this paradigm of combining the residual temperature

correction and scattering correction is not limited to the Zaneveld et al. (1994) scattering correction used here, but it could be adapted to other scattering correction methods, such as McKee et al. (2003), which allows for spectral dependence in the scattering phase function, or Tzortziou et al. (2006), which allows for nonzero particulate absorption in the NIR. Furthermore, the spectral matching method can also be used to correct vertical profile measurements from an ac-s.

The ΔT determined in the optimization is then used in Eq. (5) to give the corrected $a_p(\lambda)$, as well as to account for variations in particle beam attenuation resulting from residual temperature differences in absorption,

$$c_p(\lambda) = c_{p,\text{meas}}(\lambda) - \Psi_T(\lambda)\Delta T.$$

Because the ac-9 measures at only a single wavelength in the NIR (715 nm), the hyperspectral residual temperature and scattering correction cannot be employed. Thus, particulate spectra for the ac-9 are taken only for the TSW that is measured immediately following FSW in order to minimize the ΔT resulting from environmental variability. For example, the valve could be switched to FSW for 5 out of every 10 min, and a single set of particulate spectra would be calculated for the first stable TSW measurements after the FSW to TSW transition. Additional uncertainty in temperature results in a bias of NIR absorption $\Delta a_p(715) = \Psi_T(715)\Delta T$, which, when propagated through scattering correction, gives $\Delta a_p(\lambda) = \Psi_T(715)\Delta T[b_p'(\lambda)/b_p'(715)]$. Assuming that the spectral slope of scattering is no steeper than -1, the maximum uncertainty in absorption for the ac-9 is at 412 nm, $\Delta a_p(412) = \Psi_T(715)(412/715)^{-1}\Delta T \approx 0.006\Delta T$, and smaller for other wavelengths.

e. Filter-pad spectrophotometric particulate absorption measurements

As a validation to our approach, we compare the absorptions obtained by the in-line system ac meter to discrete water samples that were collected periodically from the flow-through system and processed for spectrophotometric particulate absorption analysis using the quantitative filter-pad method (Mitchell 1990; Bricaud and Stramski 1990; Roesler 1998). Typically, 1000 ml of seawater from the flow-through system were collected and filtered through Whatman GF/F glass fiber filters (with a nominal pore size of 0.7 μm). Filtered samples were stored in liquid nitrogen until they were shipped back to the laboratory for spectrophotometric analysis. A Cary 3E UV–visible (VIS) Spectrophotometer was used to measure optical density D_p over the wavelength range of 300–800 nm. Initially, particulate absorption was calculated as

$$a_p(\lambda) = 2.303[D_p(\lambda) - \langle D_p\rangle_{750-800}]\frac{A_{\text{eff}}}{\beta V_{\text{filt}}}, \quad (7)$$

where the factor of 2.303 accounts for the difference in the logarithm base between the Beer–Lambert law and the definition of inherent optical properties, and V_{filt} and A_{eff} are the volumes of the sample filtered and effective area of the filter pad, respectively. The effect of scattering losses on the filter pad was accounted for by subtraction of a spectrally flat baseline; here, the average of the optical density spectra over the wavelength range of 750–800 nm $\langle D_p\rangle_{750-800}$. The pathlength amplification factor β accounts for the difference in photon pathlength through the sample on a filter pad versus in suspension, for which Roesler (1998) derived a theoretical value of 2. However, because the measured optical densities from these samples were less than $O(0.1)$, the $\beta = 2$ factor derived by Roesler may not apply because the variability in the optical properties of the filter pad, rather than the sample, dominate the pathlength amplification factor. We found the empirical power-law β correction of Bricaud and Stramski (1990) to better fit the ac-9 measurements,

$$\beta(\lambda) = 1.63D_p(\lambda)^{-0.22}; \quad (8)$$

but, it is important to note that uncertainty in $\beta(\lambda)$ is a dominant source of error in calculating $a_p(\lambda)$ at low filter loadings, and that the spectrally flat scattering correction is used because no information on the spectrum of scattering is available [unlike the ac instruments, e.g., Eq. (2)].

3. Results

a. Residual temperature correction

To investigate the proposed residual temperature correction, one-fifth of the 1-min binned spectra collected during 1 day of a cruise in the equatorial Pacific (Equatorial Box Project, the R/V *Ka'imimoana* GP5-06) is presented in Fig. 3. The traditional correction based on independently measured temperature and salinity data increases the variance in the a_p spectra when compared to a simple scattering correction (Figs. 3b,c), suggesting that the temperature and salinity measurements are not sufficiently accurate for correcting the optical measurements. On the other hand, the proposed correction for residual temperature differences reduces the variance of the a_p spectra and provides a_p values that are always positive in the visible region (Fig. 3d).

The frequency distributions of the observed and estimated ΔT are presented in Fig. 4 as a further test of the

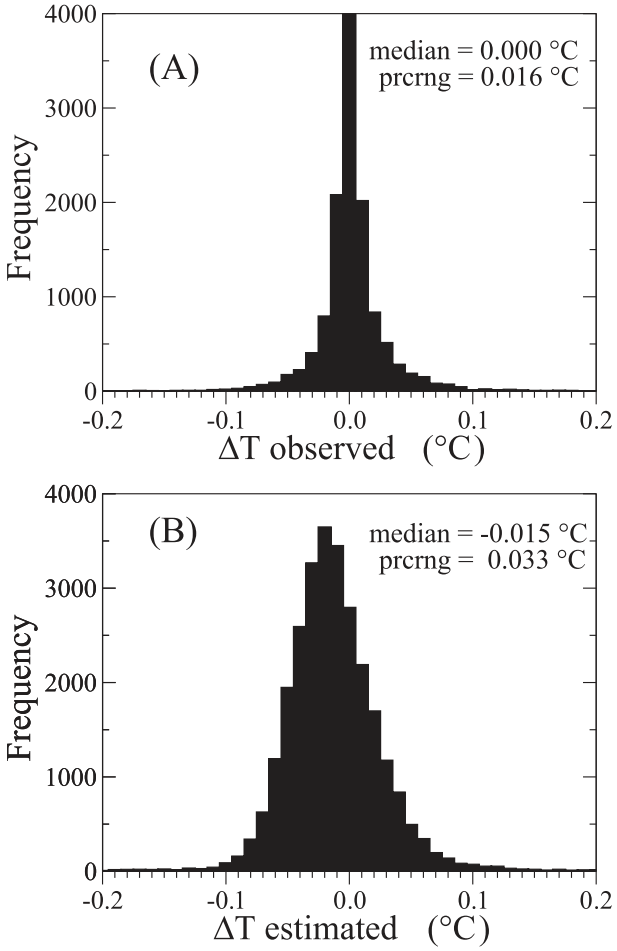

FIG. 4. (a) Frequency distribution of the measured ΔT from the temperatures obtained by interpolating between hourly adjacent measurements. (b) ΔT obtained by minimizing Eq. (6); "prcrng" is half the difference between the 84th and 16th percentiles, which is approximately one standard deviation for normally distributed data.

proposed methodology. The observed ΔT (Fig. 4a) are obtained by computing the deviations between measured temperatures (using the flow-through TSG) and temperatures obtained by linearly interpolating pairs of hourly adjacent temperature measurements. The estimated ΔT (Fig. 4b) were obtained by minimizing Eq. (6) (note that the observed ΔT are derived from the same data that failed to correct the a_p spectra satisfactorily). The frequency distribution of the estimated ΔT does not exactly overlap the distribution of the observed ΔT. Nevertheless, the agreement between the observed and estimated ranges of ΔT is remarkable, if one considers that the estimated ΔT are obtained by using the temperature effect on the measured spectra, without the use of a temperature-sensing device. The basis for the slight negative bias is unresolved, but may be due to temporal drift in the ship thermosalinograph, or real differences in water temperature reflecting the physical separation of the ac-s and TSG in the flow-through system. It should be noted that the scale of the absorption shown in the insets of Figs. 3b–d is 0.002 m^{-1}, which is near the specified precision of the ac-s (± 0.001 m^{-1} is typical and 0.003 m^{-1} is the maximum at a 4-Hz sampling rate, for wavelengths >450 nm) and is one-fifth of the specified accuracy of the instrument (± 0.01 m^{-1}). Also, the spectra are much smoother than those typically obtained from filter-pad measurements on a bench-top spectrophotometer. These appealing characteristics result primarily from the computation of each a_p spectrum as a difference of whole seawater and interpolated 0.2-μm filtered measurements.

b. Comparison with filter-pad measurements

A linear relationship is found between the filter-pad and ac-9 absorption data (440 nm, data are from the Equatorial Box Project, R/V *Ka'imimoana* GP5-05 and GP1-06) using either $\beta = 2$ of Roesler (1998; $R^2 = 0.78$, rmse = 0.0609 m^{-1}) or the empirical β of Bricaud and Stramski (1990; $R^2 = 0.77$, rmse = 0.0174 m^{-1}; see also Fig. 5). The regression offset between the ac-9 and filter-pad absorption was zero within the precision of the ac-9 for each of the two β correction methods (0.0016 and 0.0038 m^{-1} for the $\beta = 2$ and empirical β corrections, respectively). However, the regression for $\beta = 2$ had a slope of 0.54 (Fig. 5a), compared to the empirical β slope of 0.68 (Fig. 5b).

While the agreement between the filter-pad and flow-through ac-9 is good, we suspect the following four factors contributed to the regression slopes that are different from unity (black lines in Fig. 5): 1) differences in the filtration method between the ac-9, with a high-throughput 0.2-μm membrane cartridge filter and the spectrophotometric approach utilizing 0.7-μm nominal pore size GF/F filter pads; 2) uncertainty in the β correction; 3) a wider spectral bandwidth [full width at half maximum (FWHM)] of the ac-9 instrument (10 nm) compared to the bench-top spectrophotometer (2 nm), resulting in a flattening of the absorption peaks with the ac-9; and 4) uncertainty in the scattering corrections for ac-9 and filter-pad data. Despite these differences, the consistency in the measurements throughout the cruises supports the use of the filtered–unfiltered technique to obtain high-quality particulate absorption spectra.

c. Example 1: Equatorial transect

As an example of the presented method, Fig. 6 shows measurements made during a north–south transect along 125°W from approximately 8°N to 8°S (R/V *Ka'imimoana* GP5-06) as part of the Equatorial Box Project (Dall'Olmo et al. 2009; Behrenfeld et al. 2006). Figure 6a shows several

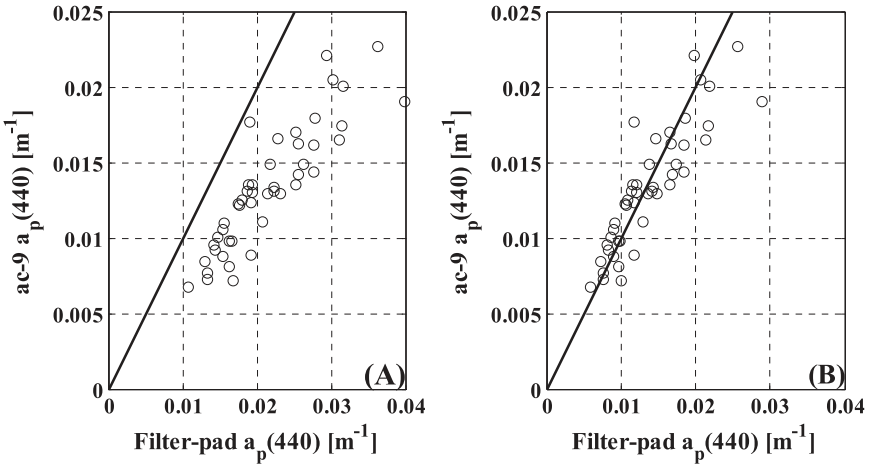

FIG. 5. Comparison of $a_p(\lambda)$ determined by flow-through ac-9 and filter-pad measurements. Data are shown for measurements made at 440 nm for two different β correction methods: (a) for the Roesler (1998) $\beta = 2$ correction, and (b) for the Bricaud and Stramski (1990) empirical correction. Black lines denote a 1:1 relationship.

hours of raw measured absorption data from the 25-cm pathlength ac-s, including periodic (hourly) filtered measurements. Raw data were binned and filtered measurements were linearly interpolated and subtracted from unfiltered water measurements, yielding the calibration-independent particulate spectra that could then be corrected for scattering and residual temperature as described in the section 2d, the result of which is shown in Fig. 6b. Variation in a_p(442 nm) over the entire transect is slightly greater than 0.01 m^{-1}. However, smaller-scale absorption features of the order of 0.005 m^{-1} are also observed over time scales of order 1 h or space scales of roughly 10 km. These features are at the limit of the factory-specified accuracy of the instrument because of calibration and correction uncertainties, yet are well resolved using the differencing approach described herein. The observed finescale variations are attributable to small-scale patchiness in surface particulate matter distribution [spatial variations in dissolved material are usually significantly smaller, as inferred from filtered segments, and are monitored using an in-line dissolved organic matter (DOM) fluorometer].

Spectral slopes of particulate beam attenuation are calculated as power-law fits to $c_p(\lambda) \propto \lambda^{-\gamma}$ as estimates of size distribution tendencies (Boss et al. 2001). Overall, the high values of γ over this transect (Fig. 6c) suggest a suspension dominated by small particles. Continuous measurement of optical properties over a multiday time series showcases a strong diel component in the particle size distribution slope, possibly resulting from cell division (e.g., Cullen and Lewis 1995; Vaulot et al. 1995), and a sharp front near the equator (crossed at 1842 UTC 30 August 2006) with strong shift in particle size corresponding with a cold front observed in the SST data (Fig. 6d).

d. *Example 2: Bottom boundary layer tripod deployment*

As a second example of the presented method, Fig. 7 shows measurements collected for nearly 20 days in September 2005, with instrumentation deployed on a bottom-mounted tripod sampling at approximately 1.2 m above the bottom in 12-m water depth at the Woods Hole Oceanographic Institution MVCO. Particulate beam attenuation in this environment, measured by a 10-cm-pathlength ac-9, ranged from approximately 1 to 20 m^{-1} (Fig. 7a), with a dynamic range in optical properties driven by strong tides, ongoing destratification, and two large storms affecting the region [Hurricane Irene (approximately yearday 250–252) that passed far offshore, but strongly increased wave forcing (data not shown); Tropical Storm Ophelia (approximately yearday 258–260) passed very close to MVCO]. Cartridge filters were replaced by divers on yeardays 252 and 262 (denoted by dashed vertical lines in Fig. 7).

Measurements of raw filtered absorption (Fig. 7b) exhibit a largely constant monotonic increase in absorption (also in attenuation, data are not shown) over the deployment, which is likely due to biofouling of the optical windows in the ac-9 (Manov et al. 2004). The increase near yearday 262 is associated with an advective feature bringing increased colored dissolved organic material to the study site. Our confidence in long-term data quality is increased as we see continuity in the spectral slope of the particulate beam attenuation γ (see Fig. 7c) both before

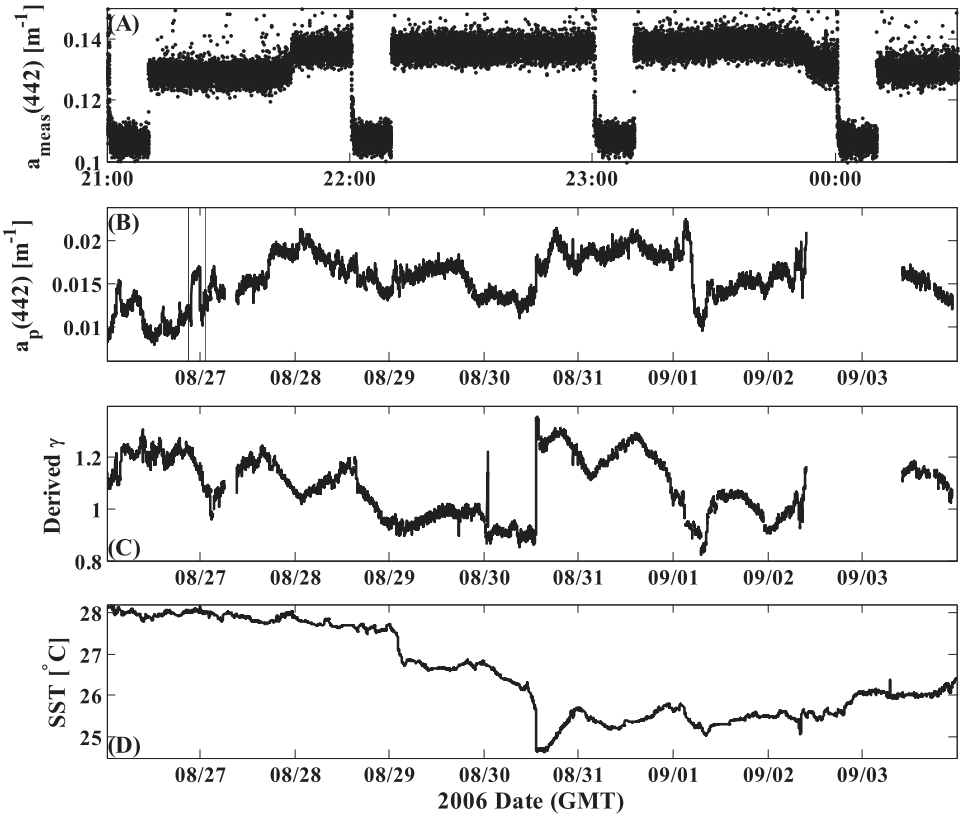

FIG. 6. Time series of particle absorption and attenuation measured during a transect crossing the equator at 125°W. (a) Four hours of high-resolution ac-s data from 27 Aug 2006 show periodic FSW measurements, which are interpolated and subtracted from TSW data. (b) Computed a_p data for whole transect. (c) Relative changes in particle size as indicated by γ exhibit a diel pattern indicative of cell growth and division and (d) a distinct front corresponding to SST data.

and after changes in the filter. If filter clogging and fouling were biasing our measurements, we would expect a transient in γ after the filter change, especially because of the expected sensitivity of γ to small particles that are likely to grow within the filter. Changes in the effective pore size of the filter resulting from clogging would also likely result in an increasing bias of γ as filters age. Figure 7d shows the measured flow rate during the filtered samples. At the beginning of the deployment, the system with a new filter achieved flow rates of $\sim$2 l min^{-1}. Clogging of the filter over time was apparent, but flow rates of $\sim$2 l min^{-1} were restored after replacing the filter. Between yeardays 252 and 262, flow rates decreased and asymptotically approached a value of approximately 0.7 l min^{-1}. Sporadic reductions in flow rate are also visible in the time series and likely were due to the turbine-style flow sensors that are used in early versions of the system. Turbine flow sensors are not compatible with particulate-laden suspensions and accordingly they have been replaced with paddlewheel-style sensors in more recent versions of the underway system.

4. Discussion

Implementation of either the moored or underway systems described here requires consideration of a number of factors, specifically, the logistical limitations of the field work at hand, and the frequency of filter samples, filter replacement, and filter cleaning. For example, in general there are no simple rules for determining how often the cartridge filter should be replaced. Instead, the replacement frequency is likely to be determined in part by the logistics of the diver operations or instrument recovery and redeployment in the case of a mooring, or as a consequence of available technician time and ease of access to the instrumentation package in the case of an underway system. In either situation, the expected lifetime of a filter is also dependent on the environment that is being observed (e.g., turbid waters clog cartridge filters faster than oligotrophic waters). The frequency of filtered measurements also impacts filter lifetime, with more frequent filtered measurements causing more rapid clogging. We typically replace cartridge filters in

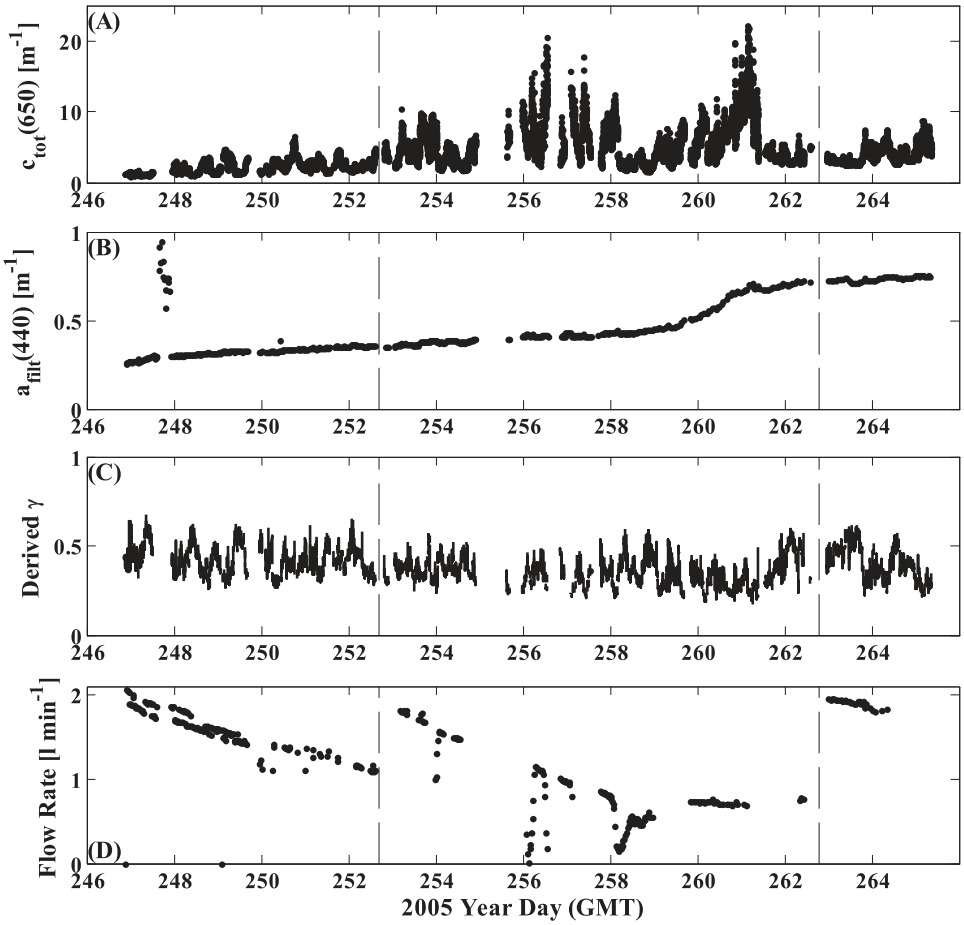

FIG. 7. Raw time series of (a) measured total attenuation and (b) filtered absorption. (c) Particle size as indicated by γ derived from spectral beam attenuation. (d) Measured flow rate during the periodic filtered samples (some data are missing resulting from the logging malfunction). Dashed vertical lines denote filter cartridge replacement by divers.

underway systems from once per week to once every other week, and we designed our moored systems in turbid waters for weekly replacement by divers. In both cases, we find no evidence of degradation (e.g., based on continuity of γ and a_{filt} before and after filter changes) in measurement quality resulting from filter overloading, even when filters were left in place for longer than 1 week at ~1 m above the bottom in a turbid bottom boundary layer (Fig. 7). In some environments with significant particle loads, using an additional, coarser (e.g., 5 μm) prefilter could prolong the life of the more expensive submicron filters.

The significant reduction in flow rate over time for the turbid bottom boundary layer measurements (Fig. 7c) indicates that significant material was retained on and within the filter. Before deploying the system for the first time, we expected to see decreases in filtered absorption after the replacement of the cartridge filters, suspecting the filter (and the biological community making it their home) to be a source of dissolved organic matter. The data shown in Fig. 7b do not support this hypothesis. After the first filter replacement, a small decrease in filtered absorption is found [$\Delta a_{\text{filt}}(440) \sim 0.005$ m^{-1}], while after the second filter change no difference is evident. This is most likely due to the large volume of water flushing the filter. Bacterial film grown on the optical surfaces of the ac instruments would lead to a decrease in transmission through optical windows, as well as a decrease in the reflectance of the absorption tube. This could result in an increase in measured absorption, as well as a decrease in instrument sensitivity.

The utility of underway measurement systems has already been demonstrated in examining processes over large spatial and long temporal scales (Colebrook 1979; Balch et al. 2004; Holley and Hydes 2002; Kirkpatrick et al. 2003) and the technology has now matured to the

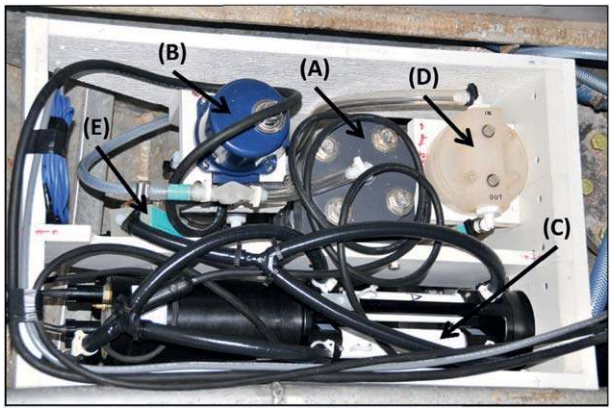

FIG. 8. Flow through installed in the bilge of R/V *Tara*, at the time of this writing underway on 3-yr mission to measure ocean properties. Flowing seawater enters system at (a) a Vortex debubbler, before (b) the three-way electrically actuated valve, which sends flow directly to (c) the ac-s instrument, or diverts it through (d) a 0.2-mm cartridge filter, before entering the ac-s instrument. Seawater flow is measured using (e) a paddle-wheel flow sensor. The valve controller and logging computer are located in dry laboratory space.

point that FerryBox and other underway systems measure not only typical physical parameters, such as temperature and salinity, but also pH, turbidity, dissolved organic, chlorophyll fluorescence, and pCO_2 (FerryBox 2009; Dandonneau 1995). Sensor maintenance and calibration is largely automated using the injection of cleaning agents and clean water into the flow stream (Kirkpatrick et al. 2003). While the technology has improved, high-accuracy optical measurements have proved difficult to obtain (FerryBox 2009) in such systems. The exciting potential in the method presented here is not only in short deployments of a few weeks, as described, but also in longer-term seasonal and multiyear automated deployments. Currently, we have installed a flow-through system with an ac-s onboard the R/V *Tara* (information available online at http://oceans.taraexpeditions.org), a sailing research vessel that has recently embarked on a 3-yr around-the-world mission to measure ocean properties (Fig. 8). Currently, the system is being maintained (approximately weekly cleaning and filter replacement) by ship technicians. One can envision, however, a system with filter banks that is able to automatically switch to a new filter on a schedule or when the current filter is sufficiently fouled (e.g., for remote mooring applications). The system would also benefit from a cleaning cycle such as that used in the FerryBox systems. Using the periodic measurement of ''pure'' water would also allow for quantitative measurements of dissolved absorption. Such a system would be able to make unattended measurements on vessels of opportunity or moorings for several months.

5. Summary

Acquiring in situ particulate absorption data from a shipboard flow-through system in clear open-ocean waters is difficult when absorption values are of the same order of magnitude as the uncertainty in pure water calibrations. Proper pure water instrument calibrations at sea are challenging and rarely conducted at a sufficient frequency to correct for effects of instrument fouling and drift. By taking the difference between temporally adjacent total and filtered seawater measurements with a switchable 0.2-μm filter cartridge, we produced absorption spectra that are within the resolution of the instrument and are independent of clear water calibrations, offsets resulting from drift in instrument electronics or optics, fouling of optical windows, and, in principle, temperature and salinity correction. However, because sample temperatures vary between whole and filtered water measurements, a residual temperature correction is needed to account for this ΔT, especially in clear waters where sample temperature data with accuracy better than ~0.05°C are needed for scattering correction of absorption data.

Here we described a methodology for scattering correction needing only measured hyperspectral absorption spectra. The technique makes use of spectral matching between observations and the expected effect of temperature on pure water absorption to derive the unknown ΔT. Results show that a_p spectra processed in this way are more physically realistic than those obtained by applying the traditional temperature and salinity correction.

We have also shown that data collected with an ac-9 using the difference method are consistent with discrete filter-pad particulate absorption analysis calculated in the laboratory using a spectrophotometer. The flow-through differencing technique allows measurements of particulate optical properties at high sample rates over a variety of time and space scales and at the limit of ac-9 accuracy. Having the ability to make such measurements in a wide range of waters, from optically clear to turbid nearshore waters, at high temporal and spatial resolution, will improve our ability to resolve small-scale structure in the open ocean, as well as collect large datasets needed for validation of ocean color remote sensing and biogeochemical models.

Acknowledgments. We thank the captain and crew of the R/V *Ka'imimoana* for making the Equatorial Box Project possible; John Trowbridge, Janet Fredericks, Jay Sisson, Stephen Faluotico, Andrew Girard, and others at the WHOI Applied Ocean Physics and Engineering Department for supporting our efforts at the WHOI

Martha's Vineyard Coastal Observatory; and also James Sullivan and two anonymous reviewers for insightful comments on an earlier draft. This work was funded through grants by the National Aeronautics and Space Administration Ocean Biology and Biogeochemistry Program (NS161A-C) and the Office of Naval Research Environmental Optics program (N00014-04-1-0235).

REFERENCES

Ainsworth, C., 2008: FerryBoxes begin to make waves. *Science,* **322,** 1627–1629.

Babin, M., and D. Stramski, 2002: Light absorption by aquatic particles in the near-infrared spectral region. *Limnol. Oceanogr.,* **47,** 911–915.

Balch, W., D. Drapeau, B. Bowler, E. Booth, J. Goes, A. Ashe, and J. Frye, 2004: A multi-year record of hydrographic and bio-optical properties in the Gulf of Maine: I. Spatial and temporal variability. *Prog. Oceanogr.,* **63,** 57–98.

Behrenfeld, M. J., and E. Boss, 2003: The beam attenuation to chlorophyll ratio: An optical index of phytoplankton photoacclimation in the surface ocean? *Deep-Sea Res. I,* **50,** 1537–1549.

——, K. Worthington, R. M. Sherrell, F. Chavez, P. Strutton, M. McPhaden, and D. Shea, 2006: Controls on tropical Pacific Ocean productivity revealed through nutrient stress diagnostics. *Nature,* **442,** 1025–1028.

Bishop, J. K. B., 1999: Transmissometer measurement of POC. *Deep-Sea Res. I,* **46,** 353–369.

Boss, E., and J. R. V. Zaneveld, 2003: The effect of bottom substrate on inherent optical properties; evidence of biogeochemical processes. *Limnol. Oceanogr.,* **48,** 346–354.

——, M. Twardowski, and S. Herring, 2001: Shape of the particulate beam attenuation spectrum and its inversion to obtain the shape of particulate size distribution. *Appl. Opt.,* **40,** 4885–4893.

——, R. Collier, G. Larson, K. Fennel, and W. S. Pegau, 2007: Measurements of spectral optical properties and their relation to biogeochemical variables and processes in Crater Lake National Park, OR. *Hydrobiologia,* **574,** 149–159.

Bricaud, A., and D. Stramski, 1990: Spectral absorption coefficients of living phytoplankton and non-algal biogenous matter: A comparison between the Peru upwelling area and Sargasso Sea. *Limnol. Oceanogr.,* **35,** 562–582.

——, A. Morel, M. Babin, K. Allali, and H. Claustre, 1998: Variations in light absorption by suspended particles with chlorophyll a concentration in oceanic (case 1) waters: Analysis and implications for biooptical models. *J. Geophys. Res.,* **103,** 31 033–31 044.

Colebrook, J. M., 1979: Continuous plankton records: Seasonal cycles of phytoplankton and copepods in the North Atlantic ocean and the North Sea. *Mar. Biol.,* **51,** 23–32.

Cullen, J. J., and M. R. Lewis, 1995: Biological processes and optical measurements near the sea surface: Some issues relevant to remote sensing. *J. Geophys. Res.,* **100,** 13 255–13 266.

Dall'Olmo, G., T. K. Westberry, M. J. Behrenfeld, E. Boss, and W. H. Slade, 2009: Significant contribution of large particles to optical backscattering in the open ocean. *Biogeosciences,* **6,** 947–967.

Dandonneau, Y., 1995: Sea-surface partial pressure of carbon dioxide in the eastern equatorial Pacific (August 1991 to October 1992): A multivariate analysis of physical and biological factors. *Deep-Sea Res. II,* **42,** 349–364.

Eisner, L., M. S. Twardowski, T. J. Cowles, and M. J. Perry, 2003: Resolving phytoplankton photoprotective:photosynthetic carotenoid ratios on fine scales using in situ spectral absorption measurements. *Limnol. Oceanogr.,* **48,** 632–646.

FerryBox, cited 2009: Sensors used in FerryBox systems. FerryBox Community. [Available online at http://www.ferrybox.org/ferry_box/sensors/.]

Fujii, M., E. Boss, and F. Chai, 2007: The value of adding optics to ecosystem models: A case study. *Biogeosciences,* **4,** 817–835.

Gardner, W. D., I. D. Walsh, and M. J. Richardson, 1993: Biophysical forcing of particle production and distribution during a spring bloom in the North Atlantic. *Deep-Sea Res. II,* **40,** 171–195.

Holley, S., and D. J. Hydes, 2002: ''Ferry-Boxes'' and data stations for improved monitoring and resolution of eutrophication related processes: Application in Southampton Water UK a temperate latitude hypernutrified estuary. *Hydrobiologia,* **475–476,** 99–110.

Kirkpatrick, G. J., C. Orrico, M. A. Moline, M. Oliver, and O. M. Schofield, 2003: Continuous hyperspectral absorption measurements of colored dissolved organic material in aquatic systems. *Appl. Opt.,* **42,** 6564–6568.

Manov, D., G. Chang, and T. Dickey, 2004: Methods for reducing biofouling of moored optical sensors. *J. Atmos. Oceanic Technol.,* **21,** 958–968.

McKee, D., A. Cunningham, and S. Craig, 2003: Semi-empirical correction algorithm for AC-9 measurements in a coccolithophore bloom. *Appl. Opt.,* **42,** 4369–4374.

Mitchell, B. G., 1990: Algorithms for determining the absorption coefficient for aquatic particulates using the quantitative filter technique. *Ocean Optics X,* R. W. Spinrad, Ed., International Society for Optical Engineering (SPIE Proceedings, Vol. 1302), 137–148.

Moore, C., E. J. Bruce, W. S. Pegau, and A. D. Weidemann, 1997: WETlabs ac-9: Field calibration protocol, deployment techniques, data processing, and design improvements. *Ocean Optics XIII,* S. G. Ackleson, Ed., International Society for Optical Engineering (SPIE Proceedings, Vol. 2963), 725–730.

Mueller, J. L., R. W. Austin, A. Morel, G. S. Fargion, and C. R. McClain, 2003: Ocean optics protocols for satellite ocean color sensor validation, revision 4, volume I: Introduction, background and conventions. NASA Goddard Space Flight Center Tech. Memo NASA/TM-2003-21621/Rev-Vol I, 56 pp. [Available online at http://oceancolor.gsfc.nasa.gov/DOCS/Protocols_Ver4_VolI.pdf.]

Pegau, W. S., and J. R. V. Zaneveld, 1993: Temperature-dependent absorption of water in the red and near-infrared portions of the spectrum. *Limnol. Oceanogr.,* **38,** 188–192.

——, and ——, 1994: Temperature dependence of the absorption coefficient of pure water in the visible portion of the spectrum. *Ocean Optics XII,* J. S. Jaffe, Ed., International Society for Optical Engineering (SPIE Proceedings, Vol. 2258), 597–604.

Peterson, R. E., 1978: A study of suspended particulate matter: Arctic Ocean and northern Oregon continental shelf. Ph.D. thesis, Oregon State University, 134 pp.

Roesler, C., 1998: Theoretical and experimental approaches to improve the accuracy of particulate absorption coefficients derived from the quantitative filter technique. *Limnol. Oceanogr.,* **43,** 1649–1660.

Roesler, C. S., and E. Boss, 2008: In situ measurement of the inherent optical properties (IOPs) and potential for harmful algal bloom detection and coastal ecosystem observations. *Real-Time Coastal Observing Systems for Ecosystem Dynamics and*

Harmful Algal Blooms, M. Babin, C. S. Roesler, and J. J. Cullen, Eds., UNESCO Publishing, 153–206.

Schofield, O., T. Bergmann, M. Oliver, A. Irwin, G. Kirkpatrick, W. P. Bissett, M. A. Moline, and C. Orrico, 2004: Inversion of spectral absorption in the optically complex coastal waters of the Mid-Atlantic Bight. *J. Geophys. Res.,* **109,** C12S04, doi:10.1029/2003JC002071.

Sullivan, J., M. Twardowski, J. R. V. Zaneveld, C. Moore, A. Barnard, P. Donaghay, and B. Rhoades, 2006: Hyperspectral temperature and salt dependencies of absorption by water and heavy water in the 400–750 nm spectral range. *Appl. Opt.,* **45,** 5294–5309.

Twardowski, M. S., J. M. Sullivan, P. L. Donaghay, and J. R. V. Zaneveld, 1999: Microscale quantification of the absorption by dissolved and particulate material in coastal waters with an ac-9. *J. Atmos. Oceanic Technol.,* **16,** 691–707.

Tzortziou, M., J. R. Herman, C. L. Gallegos, P. J. Neale, A. Subramaniam, L. W. Harding Jr., and Z. Ahmad, 2006: Bio-optics of the Chesapeake Bay from measurements and radiative transfer closure. *Estuarine Coastal Shelf Sci.,* **68,** 348–362.

Vaulot, D., D. Marie, R. J. Olson, and S. W. Chisholm, 1995: Growth of *Prochlorococcus,* a photosynthetic prokaryote, in the equatorial Pacific Ocean. *Science,* **268,** 1480–1482.

Westberry, T. K., G. Dall'Olmo, E. Boss, M. J. Behrenfeld, and T. Moutin, 2010: Coherence of particulate beam attenuation and backscattering coefficients in diverse open ocean environments. *Opt. Express,* **18,** 15 419–15 425.

WET Labs, 2009: Ac meter protocol document (Revision P). WETLabs, Inc., 55 pp. [Available online at http://www.wetlabs.com/products/pub/ac9/acprotp.pdf.]

Zaneveld, J. R. V., and W. S. Pegau, 2003: Robust underwater visibility parameter. *Opt. Express,* **11,** 2997–3009.

——, J. Kitchen, and C. Moore, 1994: Scattering error correction of reflecting tube absorption meter. *Ocean Optics XII,* J. S. Jaffe, Ed., International Society for Optical Engineering (SPIE Proceedings, Vol. 2258), 44–55.